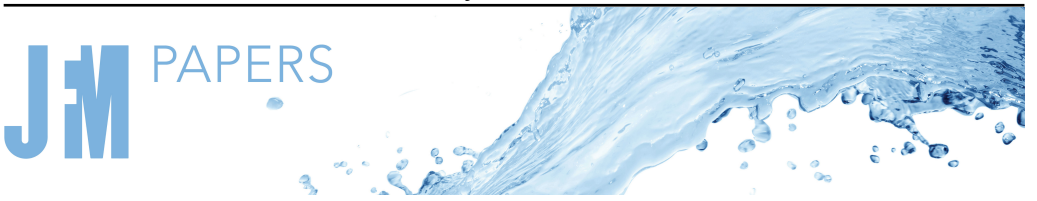
J. Fluid Mech. (2026), *vol.* 1037, A50, doi:10.1017/jfm.2026.11706



Spiral waves in water

Mark Jay Ablowitz[1], **Justin T. Cole**[2] **and Sean David Nixon**[1]

[1]Department of Applied Mathematics, University of Colorado, Boulder, CO 80309-0526, USA

[2]Department of Mathematics, University of Colorado Colorado Springs, Colorado Springs, CO 80918, USA

Corresponding author: Sean David Nixon, sean.d.nixon@gmail.com

(Received 21 August 2025 UTC; revised 11 May 2026 UTC; accepted 13 May 2026 UTC)

Spiral waves are found in linear and weakly nonlinear irrotational water-wave equations. These unsteady spiral waves evolve from suitable initial conditions; they are not induced by external forcing. In the linear case, a long-time asymptotic result is obtained via the method of stationary phase. The asymptotic approximation is found to be in good agreement with the exact solution and reveals hyperbolic spiral structure. Numerical simulations show that these spiral waves persist in the presence of weak nonlinearity. While spiral waves are frequently found in excitable media governed by reaction–diffusion systems, they comprise a new class of interesting two-space one-time dimensional phenomena in fundamental linear and nonlinear dispersive wave systems.

Key words: mathematical foundations, general fluid mechanics, surface gravity waves

1. Introduction

The analytical study of classical water waves is one of the oldest subjects in applied mathematics; its origins date back to the founders of calculus and differential equations: Newton, Bernoulli, Euler, Laplace, Lagrange, Cauchy, Airy and Stokes amongst many others (see e.g. Lamb 1932; Craik 2004). Finding and understanding the properties of solutions to the water-wave equations have been central in the study of wave phenomena. In this article we study irrotational water waves with localised initial data on an unbounded domain. In the case of linear waves, the problem can be solved via Fourier transforms, where we need to obtain the underlying dispersion relation (or wave frequency) associated with a typical wave.

Asymptotic methods are useful for approximating Fourier integrals. On the other hand, various perturbation and linearisation techniques play an important role in the study

© The Author(s), 2026. Published by Cambridge University Press. This is an Open Access article, distributed under the terms of the Creative Commons Attribution licence (https://creativecommons.org/licenses/by/4.0/), which permits unrestricted re-use, distribution and reproduction, provided the original article is properly cited.

https://doi.org/10.1017/jfm.2026.11706 Published online by Cambridge University Press

of nonlinear waves. In the case of weakly nonlinear deep-water waves, Stokes (1847) obtained a relationship between the frequency and amplitude of the dominant Fourier mode of periodic travelling waves. Over one hundred years later Benjamin & Feir (1967) found that these waves are unstable. Soon afterwards, by allowing the envelope of the wave to vary slowly in space and time Zakharov (1968) and Benney & Roskes (1969) showed that the complex amplitude of the envelope satisfies two-space, one-time dimensional nonlinear Schrödinger (NLS)-type equations. The equation that Benney and Roskes found is transformable to what is often called the Davey–Stewartson equations (see Davey & Stewartson 1974; Ablowitz & Clarkson 1991). In shallow water, the dynamics is approximated by the Boussinesq equation (Boussinesq 1871) and the Benney–Luke equation (Benney & Luke 1964). From these equations, asymptotic reductions lead to the unidirectional Korteweg–de Vries (KdV) equation (Korteweg & de Vries 1895) in one-space, one-time dimension and the Kadomtsev–Petviashvili (KP) equation (see Kadomtsev & Petviashvili 1970; Ablowitz & Clarkson 1991) in two-space, one-time dimension.

Remarkably, some of these equations in unbounded domains with rapidly decaying data have multi-soliton solutions, an infinite number of conserved quantities and can be linearised: for example the KdV equation (see Gardner *et al.* 1967), the KP equation (see e.g. Ablowitz & Clarkson 1991) and the one-space, one-time dimensional NLS equation (see Zakharov & Shabat 1972). It is also noteworthy that resonant three-wave and six-wave interaction equations are also in this class of integrable systems (Ablowitz & Haberman 1975; Zakharov & Manakov 1975; Kaup 1976). Such equations arise from classical water waves (see e.g. Ablowitz, Luo & Musslimani (2023) and references therein).

As indicated above, the study of special solutions of water waves has been a major topic over the years; see e.g. Haziot *et al.* (2021) for a review of the mathematical theory of steady water waves. Some of the areas that have attracted substantial interest are: Stokes waves near maximum height (Stokes 1880; Longuet-Higgins & Fox 1977; Amick, Fraenkel & Toland 1982; Dyachenko, Lushnikov & Korotkevich 2014) and investigations of solitary and periodic waves including existence, exact solutions and computation (Beale 1977; Strauss 1977; Amick & Toland 1981; Berger & Milewski 2000; Groves 2004).

In this article, we show that there exists a novel class of two-space one-time dimensional unsteady spiral wave structures in the linear and weakly nonlinear irrotational water-wave equations. These equations are part of a class of purely dispersive wave systems, i.e. energy-preserving equations which in the linear limit have a real dispersion relation with non-constant group velocity. Spiral waves are frequently encountered in excitable media, such as reaction–diffusion systems (see e.g. Nicolis & Prigogine 1977), electric transport systems (Bode & Purwins 1995) and disease spread (Capasso & Kunisch 1988). They can also be found in a class of galaxies (Lin & Shu 1964; Shu 2016), optically active crystals (Schell & Bloembergen 1978) and more recently they were found in tunable circular Pearcey beams (Chen *et al.* 2021) and wavepacket rotation in symmetry-broken photonic lattices (Liu *et al.* 2021).

Spiral waves are not commonly known to develop in fundamental dispersive systems. Motivated by our recent studies of Klein–Gordon equations, which are related to massive Dirac systems (Ablowitz, Cole & Nixon 2025), we have found unsteady spiral waves in linear and weakly nonlinear irrotational water waves. To our knowledge, there are no earlier analytical studies of the classical water-wave equations that feature such spiral wave phenomena. Perhaps this is due to the fact that these spirals are two-space one-time dimensional structures that evolve from a certain class of initial conditions; see (3.4). While such initial conditions are elementary, they are not obvious; we were led to these

https://doi.org/10.1017/jfm.2026.11706 Published online by Cambridge University Press

initial conditions from the study of topological wave dynamics in linear and nonlinear optics (Ablowitz *et al.* 2025). It should be noted that numerous photographs were taken of spiral-type waves in the various oceanic regions by astronauts in early space flight missions. These photographs were carefully studied in Munk *et al.* (2000), where they attributed the spiral waves to horizontal shear instability modified by rotational effects. Nevertheless, the fact that the water-wave equations admit spirals without external forcing is helpful in maintaining such structures.

The rest of this paper is organised as follows. In § 2, the governing equations are given; the linear and weakly nonlinear systems are derived. In § 3, spiral waves are shown to evolve from a class of localised initial data. The linear water-wave equations are solved via Fourier transforms and an asymptotic approximation is obtained using stationary-phase methods. In § 4, the weakly nonlinear system is numerically studied and spiral waves are found to persist for a moderate size of nonlinearity. Concluding remarks are made in § 5.

2. Governing equations

Free-surface irrotational water waves with a flat bottom, depth h, satisfy the following equations in the absence of surface tension.

(i) Ideal flow:

$$\Delta\phi = 0, \quad -h < z < \eta(\boldsymbol{r}, t), \tag{2.1}$$

(ii) no flow through the bottom:

$$\frac{\partial\phi}{\partial z} = 0, \quad \text{on} \quad z = -h, \tag{2.2}$$

(iii) Bernoulli (pressure) equation:

$$\frac{\partial\phi}{\partial t} + \frac{1}{2}|\nabla\phi|^2 + \frac{1}{2}\left(\frac{\partial\phi}{\partial z}\right)^2 + g\eta = 0 \quad \text{on} \quad z = \eta(\boldsymbol{r}, t), \tag{2.3}$$

(iv) kinematic boundary condition:

$$\frac{\partial\phi}{\partial z} = \frac{\partial\eta}{\partial t} + \nabla\phi \cdot \nabla\eta, \quad \text{on} \quad z = \eta(\boldsymbol{r}, t), \tag{2.4}$$

where $\nabla = \partial_x \mathrm{i} + \partial_y \mathrm{j}$ is the transverse gradient, $\Delta = \partial_x^2 + \partial_y^2 + \partial_z^2$ is the three dimensional Laplacian and g is the acceleration due to gravity. These four equations constitute the classical equations for irrotational water waves. Here, the unknowns are: $\phi(\boldsymbol{r}, z, t)$ the velocity potential and $\eta(\boldsymbol{r}, t)$ the surface wave elevation; $\boldsymbol{r} = (x, y)$ is the set of horizontal coordinates, z is the vertical coordinate and t is time. This is a free-boundary problem for the unknowns $\phi(\boldsymbol{r}, z, t)$ and $\eta(\boldsymbol{r}, t)$.

In Ablowitz, Fokas & Musslimani (2006), the water-wave problem was reformulated as a non-local differential–integral system for two surface unknowns, $\eta(\boldsymbol{r}, t)$ and the horizontal velocity potential $q = q(\boldsymbol{r}, t) = \phi(\boldsymbol{r}, \eta(\boldsymbol{r}, t), t)$. These equations, which we will call the AFM equations, are given by

$$\iint_{\mathbb{R}^2} \mathrm{d}\boldsymbol{r} \mathrm{e}^{-i\boldsymbol{k}\cdot\boldsymbol{r}} \left(i\eta_t \cosh[k(\eta + h)] - \frac{\boldsymbol{k} \cdot \nabla q}{k} \sinh[k(\eta + h)] \right) = 0, \tag{2.5a}$$

$$q_t + \frac{1}{2}|\nabla q|^2 + g\eta - \frac{(\eta_t + \nabla q \cdot \nabla\eta)^2}{2(1 + |\nabla\eta|^2)} = 0, \tag{2.5b}$$

https://doi.org/10.1017/jfm.2026.11706 Published online by Cambridge University Press

where $k = |\boldsymbol{k}| = \sqrt{k_x^2 + k_y^2} \geqslant 0$. It is assumed that $\eta, \nabla q, q_t$ decay rapidly to zero at infinity. Equation (2.5*b*) is Bernoulli's equation on the free surface. Equations (2.5*a*)–(2.5*b*) provide an explicit formulation of the surface variables and the non-local formulation lends itself well to asymptotic calculations, such as those considered in this paper. In the infinite depth limit, $h \to \infty$, (2.5*a*) reduces to

$$\iint_{\mathbb{R}^2} \mathrm{d}\boldsymbol{r} \mathrm{e}^{-i\boldsymbol{k}\cdot\boldsymbol{r}} \mathrm{e}^{k\eta} \left(i\eta_t - \frac{\boldsymbol{k}}{k} \cdot \nabla q \right) = 0. \tag{2.6}$$

We consider the case of weakly nonlinear waves, for which it is convenient to let $\eta \to \varepsilon\eta$, $q \to \varepsilon q$ and assume $|\varepsilon| \ll 1$. Doing so, and formally expanding the hyperbolic functions in (2.5*a*) to order ε, we find: (i) for finite depth,

$$\iint_{\mathbb{R}^2} \mathrm{d}\boldsymbol{r} \mathrm{e}^{-i\boldsymbol{k}\cdot\boldsymbol{r}} \left(i\eta_t (1 + \varepsilon k \tanh(kh)\eta) - \frac{\boldsymbol{k}}{k} \cdot \nabla q (\tanh(kh) + \varepsilon k\eta) + \cdots \right) = 0, \tag{2.7}$$

and (ii) for infinite depth, or $h \to \infty$,

$$\iint_{\mathbb{R}^2} \mathrm{d}\boldsymbol{r} \mathrm{e}^{-i\boldsymbol{k}\cdot\boldsymbol{r}} \left(\left(i\eta_t - \frac{\boldsymbol{k}}{k} \cdot \nabla q \right) (1 + \varepsilon k\eta) + \cdots \right) = 0. \tag{2.8}$$

Note that these two equations differ only by simple factors. The free-surface Bernoulli equation (2.5*b*) is unchanged regardless of finite or infinite depth; this equation to order ε reads

$$q_t = -g\eta + \frac{\varepsilon}{2}\left(\eta_t^2 - |\nabla q|^2\right) + \cdots. \tag{2.9}$$

The weakly nonlinear equations are considered in more detail in § 4.

We define the Fourier and inverse Fourier transforms as

$$\hat{f}(\boldsymbol{k}) = \frac{1}{2\pi} \iint_{\mathbb{R}^2} \mathrm{d}\boldsymbol{r} f(\boldsymbol{r}) \mathrm{e}^{-i\boldsymbol{k}\cdot\boldsymbol{r}}, \tag{2.10a}$$

$$f(\boldsymbol{r}) = \frac{1}{2\pi} \iint_{\mathbb{R}^2} \mathrm{d}\boldsymbol{k} \hat{f}(\boldsymbol{k}) \mathrm{e}^{i\boldsymbol{k}\cdot\boldsymbol{r}}. \tag{2.10b}$$

Then, from (2.7) and (2.9), the linearised equations can be written as

$$i\hat{\eta}_t - \frac{\boldsymbol{k}}{k} \cdot \widehat{\nabla q} \tanh(kh) = 0 \tag{2.11a}$$

and

$$\widehat{\nabla q}_t = -g\widehat{\nabla \eta}, \tag{2.11b}$$

where $\widehat{\nabla f} = i\boldsymbol{k}\hat{f}$. Differentiating (2.11*a*) with respect to time and combining these equations leads to

$$\hat{\eta}_{tt} + \omega^2(k)\hat{\eta} = 0, \tag{2.12}$$

where $\omega(k)$ is the linear dispersion relation for two-dimensional water waves in finite depth given by

$$\omega^2(k) = gk \tanh(kh). \tag{2.13}$$

In the infinite depth limit, $h \to \infty$, the dispersion relation is given by

$$\omega^2(k) = gk. \tag{2.14}$$

https://doi.org/10.1017/jfm.2026.11706 Published online by Cambridge University Press

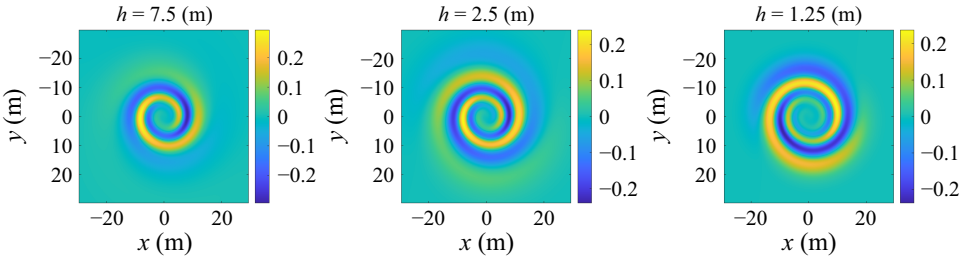


Figure 1. Evolution of the linearised water-wave equation (2.12) with dispersion relation (2.13) for initial conditions (3.1). Here $t = 5$ s, $g = 9.8\ \mathrm{m\,s^{-2}}$, $L_0 = 2.45$ m and $T_0 = 0.5$ s.

The linear surface wave $\eta(x, y, t)$ can be obtained by solving (2.12) and then taking its inverse Fourier transform. When we mention the exact solution below, this is to what we are referring.

3. Linear spiral waves

In this section, linear spiral waves are observed for certain initial conditions and analysed via the method of stationary phase. Before we do this, as an illustrative example, using Fourier transforms we solve for the wave elevation $\eta(\boldsymbol{r}, t)$ from (2.12) with the following initial conditions:

$$\eta(x, y, t = 0) = x\mathrm{e}^{-\left(\frac{r}{L_0}\right)^2}, \quad \eta_t(x, y, t = 0) = \frac{y}{T_0}\mathrm{e}^{-\left(\frac{r}{L_0}\right)^2}, \quad r^2 = x^2 + y^2, \tag{3.1}$$

where L_0 is a characteristic length scale and T_0 is a characteristic time scale. Physically, this corresponds to spatial and velocity profiles which are odd about the origin and 90° out-of-phase with each other. This configuration provides the initial 'twist' sufficient to generate spiral waves. We also find that spirals evolve from a much broader set of initial conditions of the form

$$\eta(x, y, t = 0) = P_1(x, y) f(r), \quad \eta_t(x, y, t = 0) = P_2(x, y) f(r), \tag{3.2}$$

where $P_j(x, y)$ are suitable polynomials and $f(r)$ is a rapidly decaying radially symmetric function (this is discussed further in Appendix A). We highlight the initial conditions in (3.1) due to their rather simple form that generates spiral waves.

Typical evolutions of the linear water-wave equations in dimensional units appear in figure 1 for different fluid depths. In each case, we observe two spiral arms: a (positive) arm of elevation and a (negative) arm of depression. Examining the differences, the shallower depths have more identifiable spirals, but have lost more amplitude. We do not show it here, but the finite-depth evolutions for $h > 7.5$ m converge asymptotically to the infinite-depth limit dynamics (2.14). These results clearly indicate the presence of spiral waves in linear water-wave systems. We note that these are induced by the initial conditions and not by external forcing.

Having observed these spirals numerically, we seek to describe them analytically. Here, it is convenient to transform to non-dimensional variables. This is accomplished by scaling by a characteristic length L_0, $\boldsymbol{r} \to L_0\boldsymbol{r}$, $h \to L_0 h$, chosen such that $\boldsymbol{r} \sim O(1)$, where the initial conditions are localised and characteristic time scale T_0, $t \to T_0 t$, chosen such that the non-dimensional parameter related to gravity,

$$\tilde{g} = \frac{T_0^2}{L_0} g, \tag{3.3}$$

https://doi.org/10.1017/jfm.2026.11706 Published online by Cambridge University Press

is of order 1. In the examples below we take $\tilde{g} = 1$ and use the dimensionless initial conditions

$$\eta(x, y, t = 0) = x\mathrm{e}^{-r^2}, \quad \eta_t(x, y, t = 0) = y\mathrm{e}^{-r^2}, \quad r^2 = x^2 + y^2. \tag{3.4}$$

From here on, all variables presented are non-dimensional.

Motivated by previous work used to describe spiral motion in a Klein–Gordon equation (Ablowitz *et al.* 2025), we implement the method of stationary phase to describe the structure of these spirals. The second-order linear water-wave equation (2.12) has the exact solution for decaying data

$$\eta(x, y, t) = I_+(\boldsymbol{r}, t) + I_-(\boldsymbol{r}, t), \tag{3.5}$$

where

$$\begin{aligned} I_\pm(\boldsymbol{r}, t) &= \frac{1}{2\pi} \iint_{\mathbb{R}^2} \widehat{A}_\pm(\boldsymbol{k})\, \mathrm{e}^{i(\boldsymbol{k}\cdot\boldsymbol{r} \pm \omega(k)\, t)} \mathrm{d}k_x\, \mathrm{d}k_y \\ &= \frac{1}{2\pi} \iint_{\mathbb{R}^2} \widehat{A}_\pm(\rho, \varphi)\, \mathrm{e}^{i(\rho \cos\, \varphi\, x + \rho \sin\, \varphi\, y \pm \omega(\rho)\, t)} \rho\, \mathrm{d}\varphi\, \mathrm{d}\rho. \end{aligned} \tag{3.6}$$

In the polar version of the inverse Fourier transform, we take $k_x = \rho \cos\, \varphi$ and $k_y = \rho \sin\, \varphi$. We intentionally take (ρ, φ) to denote the spectral polar coordinates to distinguish them from the standard labels (r, θ), where $x = r \cos\, \theta$, $y = r \sin\, \theta$. Notice that the dispersion relation only depends on the modulus of the Fourier wavenumbers. The coefficients $\widehat{A}_\pm$ are related to the initial conditions by

$$\widehat{A}_\pm(\rho, \varphi) = \frac{1}{2}\left(\widehat{\eta}(\rho, \varphi, 0) \pm \frac{1}{\mathrm{i}\omega(\rho)} \frac{\partial \widehat{\eta}}{\partial t}(\rho, \varphi, 0)\right), \tag{3.7}$$

where $\widehat{A}_+ = \widehat{A}_-^*$ are complex conjugates for real initial conditions. As indicated above, the long-time, $t \gg 1$, asymptotic approximation of the exact solutions is obtained through a stationary-phase analysis. This is done by first approximating in φ, then ρ. Since the dispersion relation only depends on ρ, this approach simplifies the calculation. Redefining the spatial variables, x, y, r, we create $O(1)$ variables

$$\overline{x} = \frac{x}{t}, \quad \overline{y} = \frac{y}{t}, \quad \overline{r} = \frac{r}{t}. \tag{3.8}$$

First, isolate the integral in φ:

$$J_\pm(\rho, \overline{r}, \theta, t) = \int_{-\pi}^{\pi} \widehat{A}_\pm(\rho, \varphi)\, \mathrm{e}^{i(\rho \cos\, \varphi\, \overline{x} + \rho \sin\, \varphi\, \overline{y})\, t} \mathrm{d}\varphi, \tag{3.9}$$

which has two stationary points of the Fourier phase, φ_j $j = 1, 2$, in the interval $[-\pi, \pi]$ that satisfy the equation

$$\varphi_1 = \theta, \quad \varphi_2 = \theta + \pi. \tag{3.10}$$

Here it appears that there are a total of four stationary points: two for the positive case and two for the negative. However, as we show below, only two of these values correspond to a stationary point of the solution (3.6). For the other two, the monotonicity of $\omega(\rho)$ means the phase is stationary only with respect to the angular variable, φ, but not with respect to the radial variable, ρ.

The second derivative of the phase is given by

$$\frac{\mathrm{d}^2}{\mathrm{d}\varphi^2}\big(\rho \cos\, \varphi\, \overline{x} + \rho \sin\, \varphi\, \overline{y}\big)\big|_{\varphi_j} = \rho\big(-\cos\, \varphi_j\, \overline{x} - \sin\, \varphi_j\, \overline{y}\big) \tag{3.11a}$$

$$= (-1)^j \rho\, \overline{r}. \tag{3.11b}$$

https://doi.org/10.1017/jfm.2026.11706 Published online by Cambridge University Press

Using this, we find the stationary-phase approximation:

$$J_{\pm}(\rho,\bar{r},\theta,t)\approx\sqrt{\frac{2\pi}{\rho\bar{r}\,t}}\widehat{A}_{\pm}(\rho,\varphi_1)\mathrm{e}^{i\,\rho\bar{r}\,t-i\pi/4}+\sqrt{\frac{2\pi}{\rho\bar{r}\,t}}\widehat{A}_{\pm}(\rho,\varphi_2)\mathrm{e}^{-(i\,\rho\bar{r}\,t-i\pi/4)}. \quad (3.12)$$

The integral in ρ can now be expressed as

$$\begin{aligned}I_{\pm}(\bar{r},\theta,t)&\approx\frac{1}{2\pi}\int_0^{\infty}J_{\pm}(\rho,\bar{r},t)\mathrm{e}^{\pm i\omega(\rho)t}\rho\,\mathrm{d}\rho\\&=\mathrm{e}^{-i\frac{\pi}{4}}\frac{1}{\sqrt{2\pi\bar{r}\,t}}\int_0^{\infty}\widehat{A}_{\pm}(\rho,\varphi_1)\mathrm{e}^{i\,(\rho\,\bar{r}\pm\omega(\rho))\,t}\sqrt{\rho}\,\mathrm{d}\rho\\&\quad+\mathrm{e}^{i\frac{\pi}{4}}\frac{1}{\sqrt{2\pi\bar{r}\,t}}\int_0^{\infty}\widehat{A}_{\pm}(\rho,\varphi_2)\mathrm{e}^{i\,(-\rho\,\bar{r}\pm\omega(\rho))\,t}\sqrt{\rho}\,\mathrm{d}\rho.\end{aligned} \quad (3.13)$$

Defining the phase term

$$Q_j^{\pm}(\rho,\bar{r})=(-1)^{j+1}\rho\,\bar{r}\pm\omega\big(\rho\big),\quad j=1,2, \quad (3.14)$$

the stationary points occur for values of $\bar{r}$ that satisfy

$$\frac{\mathrm{d}Q_j^{\pm}}{\mathrm{d}\rho}=(-1)^{j+1}\bar{r}\pm\frac{\partial\omega}{\partial\rho}=0. \quad (3.15)$$

For water waves, $\omega'(\rho)>0$ for $\rho>0$; thus solutions to (3.15) only occur when $j=1$ for the $-$ case or $j=2$ for the $+$ case. In either case, the radial component of the stationary point is given by

$$\bar{r}=\frac{\partial\omega}{\partial\rho}. \quad (3.16)$$

We define the solution to (3.16) as $\rho_0(\bar{r})$, which represents the only stationary point for both integrals in (3.13). Thus, stationary points of the phase in solution (3.6) occur at $(\rho_0(\bar{r}),\theta)$ and $(\rho_0(\bar{r}),\theta+\pi)$. Checking the second derivative of the phase term, we have

$$\operatorname{sgn}\left[\frac{\partial^2 Q_j^{\pm}}{\partial\rho^2}\,(\rho_0)\right]=\operatorname{sgn}\left[\pm\frac{\partial^2\omega}{\partial\rho^2}\,(\rho_0)\right]=\mp1, \quad (3.17)$$

since $\omega''(\rho)<0$. Thus, for $t\gg1$, we have the final asymptotic approximation

$$\begin{aligned}\eta(\bar{r},\theta,t)&=I_-(\bar{r},\theta,t)+I_+(\bar{r},\theta,t)\\&\approx\frac{\sqrt{\rho_0}}{\sqrt{\bar{r}\,|\omega''(\rho_0)|\,t}}\big(\widehat{A}_-(\rho_0,\varphi_1)\mathrm{e}^{i\,(\rho_0\,\bar{r}-\omega(\rho_0))\,t}+\mathrm{c.c.}\big),\\&\approx\frac{\rho_0^{3/2}\mathrm{e}^{-\frac{\rho_0^2}{4}}}{4\sqrt{\bar{r}\,|\omega''(\rho_0)|\,t}}\left[\frac{\sin\,\theta}{\omega(\rho_0)}\cos\,\big(\rho_0\,\bar{r}t-\omega(\rho_0)t\big)-\cos\,\theta\,\sin\,\big(\rho_0\,\bar{r}t-\omega(\rho_0)t\big)\right],\end{aligned} \quad (3.18)$$

where ρ_0 is the function of $\bar{r}$ that solves (3.16) and c.c. is the complex conjugate. We note that this unsteady solution decays like t^{-1} for $\bar{r}=O(1)$. This leading-order unsteady solution has three distinctive parts: (i) linear decay in time; (ii) envelope; and (iii) spiral structure inside the brackets. In general, we cannot write down an explicit formula for ρ_0 that satisfies (3.16) and instead use a numerical approximation.

https://doi.org/10.1017/jfm.2026.11706 Published online by Cambridge University Press

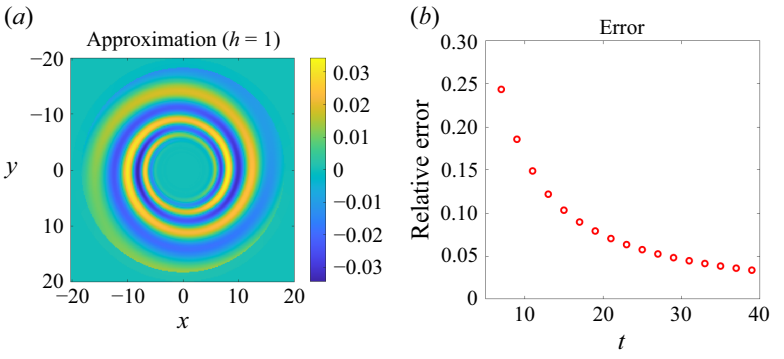


Figure 2. (*a*) Approximation given by the stationary-phase formulae (3.18) of a finite-depth spiral at $t = 20$. (*b*) Relative norm squared error (3.19) between the exact solution and the approximation is observed to converge like $O(t^{-2})$ as $t \to \infty$. For both figures $h = 1$ and $\tilde{g} = 1$.

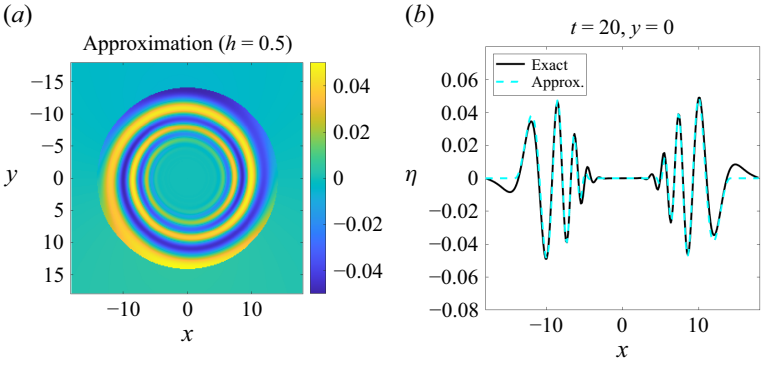


Figure 3. Approximation given by the stationary-phase formulae (3.18) of a finite-depth spiral; here $t = 20$, $h = 0.5$ and $\tilde{g} = 1$. (*a*) Contour plot. (*b*) Comparison of the solution obtained via Fourier transform, (2.12), and the approximation at cross-section $y = 0$.

A comparison between the exact solution obtained via Fourier transform from (2.12) and the stationary-phase approximation in (3.18) is shown in figures 2 and 3 (here and below in dimensionless units) for water depths of $h = 1$ and $h = 0.5$, respectively. To quantify how accurate the stationary-phase approximation is, we compute the relative norm squared error:

$$\text{Relative error} = \frac{\iint \left|\eta_{Exact} - \eta_{Approx}\right|^2 \mathrm{d}A}{\iint |\eta_{Exact}|^2 \,\mathrm{d}A}, \tag{3.19}$$

and observe that this converges like $O(t^{-2})$ as t increases. Note that the modulus of the stationary point, ρ_0, is found by numerically solving (3.16). The circumferential part, for a given $\overline{x}$, $\overline{y}$, is obtained from (3.10). We note that the approximation is valid in the domain $x^2 + y^2 < \tilde{g}ht^2$, which can be seen by noting that

$$\lim_{\rho \to 0} \frac{\mathrm{d}\omega}{\mathrm{d}\rho} = \sqrt{\tilde{g}h} \tag{3.20}$$

is the supremum of ω' for finite depth. Thus, no solution to (3.15) exists for $\overline{r} \geqslant \sup \omega'(\rho)$. Within this region, there is good agreement with the exact solution. Other integral

https://doi.org/10.1017/jfm.2026.11706 Published online by Cambridge University Press

approximations, like steepest descent, are required outside of this region. Finally, we remark that these spirals are quite robust to perturbations and persist in the nonlinear regime (as seen in § 4).

3.1. *Deep water*

Thus far, we have found an asymptotic approximation for the spiral structures, which shows that the phenomena can be expressed as a slowly varying, radially symmetric, envelope over an expression for the underlying spiral structure. In the deep-water limit, we further investigate this spiral structure to obtain a more explicit formula for the shape of the spiral expressed as r as a function of θ, which traces the path the spiral takes as it expands out from the origin. Here, as $h \to \infty$, ω is given by (2.14), or in polar form

$$\omega(\rho) = \tilde{g}^{1/2}\rho^{1/2}. \tag{3.21}$$

The equation for the stationary points, (3.16), now becomes

$$\overline{r} = \frac{1}{2}\tilde{g}^{1/2}\rho_0^{-1/2} \tag{3.22}$$

with solutions

$$\rho_0 = \frac{\tilde{g}}{4\overline{r}^2}. \tag{3.23}$$

Substituting this into (3.18), we find

$$\eta(\overline{r}, \theta, t) \approx -\frac{\tilde{g}}{t}\frac{1}{2\sqrt{2}\,\overline{r}^3}\left(\widehat{A}_-(\rho_0, \varphi_1)\mathrm{e}^{-i(\tilde{g}/4\overline{r})\,t} + \text{c.c.}\right) \tag{3.24}$$

with initial conditions (3.4) from § 2. After the Fourier coefficients in (3.7) are evaluated, we have

$$\eta(\overline{r}, \theta, t) \approx \frac{\tilde{g}^2\mathrm{e}^{-\frac{\tilde{g}^2}{64\overline{r}^4}}}{32\sqrt{2}\,\overline{r}^5\,t}\left(\frac{2\overline{r}}{\tilde{g}}\sin(\theta)\cos\left(\frac{\tilde{g}t}{4\overline{r}}\right) - \cos(\theta)\sin\left(\frac{\tilde{g}t}{4\overline{r}}\right)\right). \tag{3.25}$$

With regard to the envelope structure, we observe a dominant exponential decay to zero when $\overline{r} \to 0$, but an algebraic (quintic) decay as $\overline{r} \to \infty$. The spiral structure is further analysed in the next section.

A comparison between the exact solution obtained from (2.12) with the deep-water dispersion and the stationary-phase approximation in (3.25) is shown in figure 4. We observe that both qualitatively and quantitatively, the approximation describes the spiral wave phenomena.

3.1.1. *Deep-water spiral structure*

We now isolate the underlying spiral structure from the slowly varying envelope in order to describe the fundamental shape of the deep-water spirals. This spiral shape can be derived from (3.25). Since the surface spiral consists of regions of elevation (positive) and depression (negative), we can trace the shape of the spiral along the zeros of the solution, which occur at

$$\frac{2\overline{r}}{\tilde{g}}\sin(\theta)\cos\left(\frac{\tilde{g}t}{4\overline{r}}\right) - \cos(\theta)\sin\left(\frac{\tilde{g}t}{4\overline{r}}\right) = 0 \tag{3.26}$$

or, in terms of $r = t\overline{r}$ (see (3.8)),

$$r\tan(\theta) = \frac{\tilde{g}t}{2}\tan\left(\frac{\tilde{g}t^2}{4r}\right). \tag{3.27}$$

https://doi.org/10.1017/jfm.2026.11706 Published online by Cambridge University Press

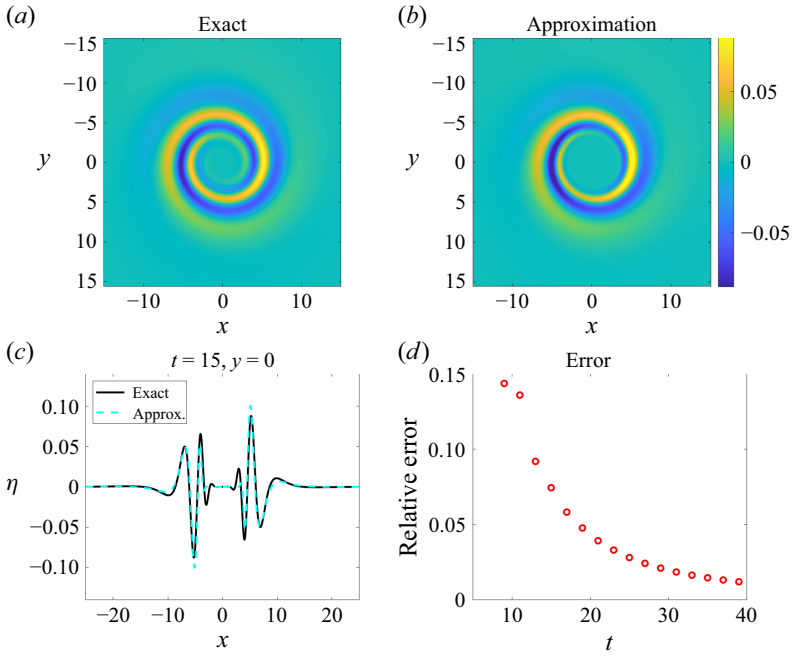


Figure 4. Comparison of the deep-water (*a*) exact solution (2.12) computed via Fourier transforms and the (*b*) approximation given by the stationary-phase formulae (3.25). (*c*) Cross-section at $y = 0$ comparing the exact solution and approximation in (*a*,*b*). (*d*) Relative norm squared error (3.19) between the exact solution and the approximation; it converges like $O(t^{-2})$ as $t \to \infty$. Here $\tilde{g} = 1$.

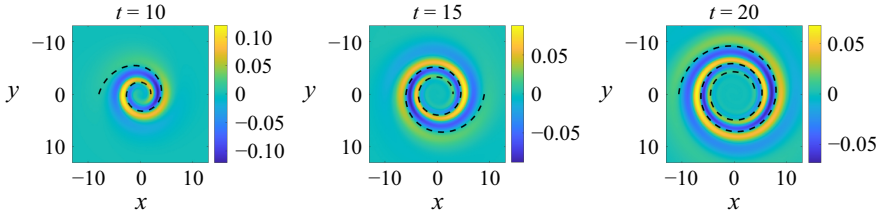


Figure 5. Comparison of the equation for the spiral shape (3.29) found in the deep-water limit (dashed line) and the exact solution obtained via Fourier transform. The black dashed curve tracks the zeros of the spiral.

To better visualise the shape of the spiral, we seek an approximate solution for r in terms of θ. If we look for the zeros ($\theta = 0$) that lie along the positive x axis, we find that nth zero has a radius of

$$\frac{\tilde{g}t^2}{4r_n} = n\pi, \quad n \in \mathbb{Z}. \tag{3.28}$$

Interpolating these zeros on the positive x axis for general θ, it suggests that the shape of the spiral is given by

$$r = \frac{\tilde{g}t^2}{4\theta}. \tag{3.29}$$

For a fixed time t, this is a hyperbolic spiral. A comparison of the curve given in (3.29) superimposed on top of the exact solution obtained from (2.12) in the deep-water limit is

https://doi.org/10.1017/jfm.2026.11706 Published online by Cambridge University Press

shown in figure 5. The curve fits the zeros of the spiral with good agreement between the two. While it is not shown here, these curves also correspond to the extrema of the surface velocity profile, $\eta_t(x, y, t)$. It is interesting to note that hyperbolic spirals have been used to describe certain galaxies where the radial spiral arm grows as it moves away from the centre (Kennicutt 1981).

4. Weakly nonlinear spiral waves

While the spiral waves discussed above are a linear phenomenon, these waves are found to be robust structures that remain intact in the presence of weak nonlinearity. Next we derive a numerical scheme for evolving spiral waves in the weakly nonlinear limit by taking the Taylor expansion of (2.5) to find suitable approximations that can be solved numerically using spectral methods to approximate the spatial derivatives and standard fourth-order Runge–Kutta methods for the time evolution. Transforming the non-local system (2.5) to non-dimensional variables and considering the amplitude limit, $\eta \to \varepsilon\eta$ and $q \to \varepsilon q$, $|\varepsilon| \ll 1$, yields

$$\iint_{\mathbb{R}^2} \mathrm{d}\boldsymbol{r}\mathrm{e}^{-i\boldsymbol{k}\cdot\boldsymbol{r}} \left(i\eta_t \cosh\left[kh + \varepsilon k\eta\right] - \frac{\boldsymbol{k}\cdot\nabla q}{k} \sinh\left[kh + \varepsilon k\eta\right] \right) = 0, \tag{4.1a}$$

$$q_t + \tilde{g}\eta + \frac{\varepsilon}{2}|\nabla q|^2 - \varepsilon \frac{(\eta_t + \varepsilon \nabla q \cdot \nabla\eta)^2}{2(1+\varepsilon^2|\nabla\eta|^2)} = 0. \tag{4.1b}$$

Then, expanding (4.1a) in powers of ε, we find

$$\begin{aligned} 0 = \widehat{\eta}_t + \tanh(kh)\frac{\mathrm{i}\boldsymbol{k}\cdot\widehat{\nabla q}}{k} + \varepsilon\left(k\tanh(kh)\widehat{\eta\eta_t} + \mathrm{i}\boldsymbol{k}\cdot\widehat{\eta\nabla q}\right) \\ + \frac{\varepsilon^2}{2}\left(k^2\widehat{\eta^2\eta_t} + k\left(\mathrm{i}\boldsymbol{k}\cdot\widehat{\eta^2\nabla q}\right)\tanh(kh)\right) + \cdots . \end{aligned} \tag{4.2}$$

In order to evolve the system, we need to solve for η_t. However, in this form, η_t is nested within the nonlinear terms. To derive a tractable weakly nonlinear system, we expand the governing equations in powers of ε and solve perturbatively for η_t:

$$\eta_t = H_0 + \varepsilon H_1 + \cdots . \tag{4.3}$$

Substituting this into (4.2) and collecting powers of ε gives

$$H_0 = -\frac{1}{2\pi}\iint_{\mathbb{R}^2} \mathrm{d}\boldsymbol{k}\mathrm{e}^{i\boldsymbol{k}\cdot\boldsymbol{r}} \tanh(kh)\frac{\mathrm{i}\boldsymbol{k}\cdot\widehat{\nabla q}}{k}, \tag{4.4a}$$

$$H_1 = -\frac{1}{2\pi}\iint_{\mathbb{R}^2} \mathrm{d}\boldsymbol{k}\mathrm{e}^{i\boldsymbol{k}\cdot\boldsymbol{r}} \left[k\tanh(kh)\widehat{\eta H_0} + \mathrm{i}\boldsymbol{k}\cdot\widehat{\eta\nabla q}\right]. \tag{4.4b}$$

Equation (4.2) may now be written in explicit terms as

$$\begin{aligned} \widehat{\eta}_t \approx -\tanh(kh)\frac{\mathrm{i}\boldsymbol{k}\cdot\widehat{\nabla q}}{k} - \varepsilon\left(k\tanh(kh)\widehat{\eta H_0} + \mathrm{i}\boldsymbol{k}\cdot\widehat{\eta\nabla q}\right) \\ - \varepsilon^2\left(k\tanh(kh)\widehat{\eta H_1} + \frac{k^2}{2}\widehat{\eta^2 H_0} + \frac{k}{2}\left(\mathrm{i}\boldsymbol{k}\cdot\widehat{\eta^2\nabla q}\right)\tanh(kh)\right), \end{aligned} \tag{4.5}$$

where we truncate the expansion at $O(\varepsilon^2)$.

https://doi.org/10.1017/jfm.2026.11706 Published online by Cambridge University Press

Applying expansion (4.3) in (4.1*b*) now gives

$$0 = q_t + \tilde{g}\,\eta + \frac{\varepsilon}{2}\left|\nabla q\right|^2 - \frac{\varepsilon}{2}\frac{\left(\eta_t + \varepsilon\nabla\eta\,\cdot\,\nabla q\right)^2}{1+\varepsilon^2\left|\nabla\eta\right|^2}, \tag{4.6a}$$

$$0 = q_t + \tilde{g}\,\eta + \frac{\varepsilon}{2}\left|\nabla q\right|^2 - \frac{\varepsilon}{2}\left(\eta_t^2 + 2\varepsilon\eta_t\nabla\eta\,\cdot\,\nabla q + \cdots\right)\left(1-\varepsilon^2\left|\nabla\eta\right|^2+\cdots\right), \tag{4.6b}$$

$$0 = q_t + \tilde{g}\,\eta + \frac{\varepsilon}{2}\left|\nabla q\right|^2 - \frac{\varepsilon}{2}\eta_t^2 - \varepsilon^2\eta_t\nabla\eta\,\cdot\,\nabla q + \cdots, \tag{4.6c}$$

$$0 = q_t + \tilde{g}\,\eta + \frac{\varepsilon}{2}\left|\nabla q\right|^2 - \frac{\varepsilon}{2}(H_0^2 + 2\varepsilon H_0 H_1) - \varepsilon^2 H_0\nabla\eta\,\cdot\,\nabla q - \cdots, \tag{4.6d}$$

where H_0 and H_1 are taken from the η_t expansion (4.4). Hence,

$$q_t \approx -\tilde{g}\,\eta + \frac{\varepsilon}{2}\left(H_0^2 - \left|\nabla q\right|^2\right) + \varepsilon^2\left(H_0 H_1 + H_0\nabla\eta\,\cdot\,\nabla q\right). \tag{4.7}$$

The final system describing the evolution of weakly nonlinear waves is given by

$$\widehat{\eta}_t \approx -\tanh(kh)\frac{\mathrm{i}\boldsymbol{k}\,\cdot\,\widehat{\nabla q}}{k} - \varepsilon\left(k\tanh(kh)\widehat{\eta H_0} + \mathrm{i}\boldsymbol{k}\,\cdot\,\widehat{\eta\nabla q}\right) - \varepsilon^2\left(k\tanh(kh)\widehat{\eta H_1} + \frac{k^2}{2}\widehat{\eta^2 H_0} + \frac{k}{2}\widehat{\left(\mathrm{i}\boldsymbol{k}\,\cdot\,\eta^2\nabla q\right)}\tanh(kh)\right), \tag{4.8a}$$

$$\left(\widehat{\nabla q}\right)_t \approx \mathrm{i}\boldsymbol{k}\left(-\tilde{g}\,\widehat{\eta} + \frac{\varepsilon}{2}\left(\widehat{H_0^2} - \widehat{\left|\nabla q\right|^2}\right) + \varepsilon^2\left(\widehat{H_0 H_1} + H_0\widehat{\nabla\eta\,\cdot\,\nabla q}\right)\right), \tag{4.8b}$$

where H_0, H_1 are given by (4.4). Or, in terms of the dispersion relation, $\omega(k)$, we can write these equations as

$$H_0 = -\frac{1}{2\pi\tilde{g}}\iint_{\mathbb{R}^2}\mathrm{d}\boldsymbol{k}\mathrm{e}^{i\boldsymbol{k}\cdot\boldsymbol{r}}\,\omega^2(k)\frac{\mathrm{i}\boldsymbol{k}\,\cdot\,\widehat{\nabla q}}{k^2}, \tag{4.9a}$$

$$H_1 = -\frac{1}{2\pi\tilde{g}}\iint_{\mathbb{R}^2}\mathrm{d}\boldsymbol{k}\mathrm{e}^{i\boldsymbol{k}\cdot\boldsymbol{r}}\left[\omega^2(k)\widehat{\eta H_0} + \mathrm{i}\tilde{g}\boldsymbol{k}\,\cdot\,\widehat{\eta\nabla q}\right], \tag{4.9b}$$

$$\widehat{\eta}_t \approx -\omega^2(k)\frac{\mathrm{i}\boldsymbol{k}\,\cdot\,\widehat{\nabla q}}{\tilde{g}k^2} - \varepsilon\left(\frac{1}{\tilde{g}}\omega^2(k)\widehat{\eta H_0} + \mathrm{i}\boldsymbol{k}\,\cdot\,\widehat{\eta\nabla q}\right) - \varepsilon^2\left(\frac{1}{\tilde{g}}\omega^2(k)\widehat{\eta H_1} + \frac{k^2}{2}\widehat{\eta^2 H_0} + \frac{1}{2\tilde{g}}\omega^2(k)\widehat{\left(\mathrm{i}\boldsymbol{k}\,\cdot\,\eta^2\nabla q\right)}\right), \tag{4.9c}$$

$$\left(\widehat{\nabla q}\right)_t \approx \mathrm{i}\boldsymbol{k}\left(-\tilde{g}\,\widehat{\eta} + \frac{\varepsilon}{2}\left(\widehat{H_0^2} - \widehat{\left|\nabla q\right|^2}\right) + \varepsilon^2\left(\widehat{H_0 H_1} + H_0\widehat{\nabla\eta\,\cdot\,\nabla q}\right)\right). \tag{4.9d}$$

We note that, to $O(\varepsilon^2)$, these equations are equivalent to those derived in Craig & Sulem (1993) where the expansion is found using the Dirichlet to Neumann operator (see e.g. Wang & Milewski 2012).

In these equations we evolve $\widehat{\eta}$, $\widehat{q_x}$ and $\widehat{q_y}$; note that the last line has ∇q, not q. This has two benefits, one physical and one numerical. First, ∇q represents the surface fluid velocity, which is an important physical quantity. Second, an important source of numerical instability arises from the high-frequency ($k \gg 1$) modes, and in this form the scaling of the nonlinear terms with respect to k is reduced in order, i.e. terms of order ε

https://doi.org/10.1017/jfm.2026.11706 Published online by Cambridge University Press

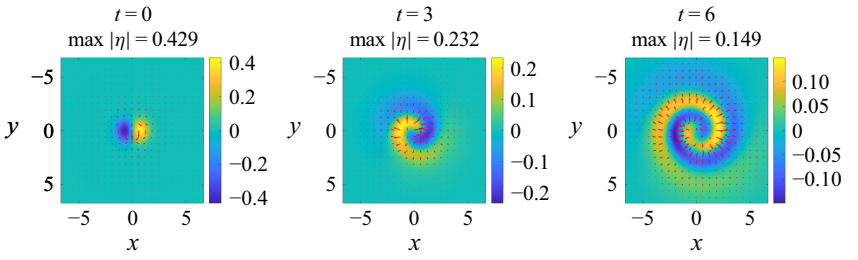


Figure 6. Evolution of the finite-depth nonlinear water-wave equations (4.8) with initial conditions (3.4). Surface velocity $\nabla q(\boldsymbol{r}, t)$ is displayed as a vector field overlaying the plot of $\eta(\boldsymbol{r}, t)$. Here $h = 1$, $\varepsilon = 0.25$ and $\tilde{g} = 1$.

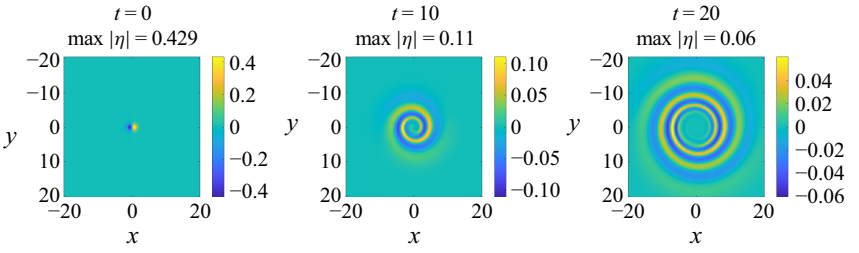


Figure 7. Evolution of the finite-depth nonlinear water-wave equations (4.8) with initial conditions (3.4). Here $\varepsilon = 0.25$, $h = 0.7$ and $\tilde{g} = 1$. This can be compared with the linear results shown in figure 3.

scale like $O(k)$ instead of $O(k^2)$ and terms of order ε^2 scale like $O(k^2)$ instead of $O(k^3)$. The numerical scheme used to solve (4.8) is a fourth-order Runge–Kutta method with integrating factor. Details are given in Appendix B.

In figure 6, we plot $\eta(\boldsymbol{r}, t)$ overlaid with the vector field defined by $\nabla q(\boldsymbol{r}, t)$; this illustrates how the initial spiral structure develops from the initial conditions (3.4). In the initial conditions, the velocity field is characterised by a sink and source that are located along the axis separating the initial regions of depression and elevation (in this example, the y axis). As the system is evolved, this sink and source begin rotating around each other. For long-time evolutions, this develops into a radially oriented velocity field that is inwardly directed for regions of depression and outwardly oriented for regions of elevation.

Using the same initial conditions (3.4) prescribed in the linear system described § 3, we find that linear spiral waves constitute a robust family of solutions and adding weak nonlinearity does not have significant impact on the formation and persistence of the spiral waves observed in the linear problem. Snapshots of the nonlinear evolution for finite-depth waves are shown in figure 7. These results can be compared against the linear evolution shown in figure 3. The difference between the two is small (see also figure 12) with the nonlinear version showing a few extra spirals near the centre and a slightly larger peak amplitude. This makes intuitive sense, since the spirals are composed of non-stationary waves and the weak nonlinearity does not grow in strength due to nonlinear feedback.

Deep-water spirals in the presence of weak nonlinearity are highlighted in figure 8. These results can be compared with the linearised version in figure 4. Comparing the two at $t = 10$, we see that the spiral phenomenon persists and the hyperbolic spiral shape, as given in § 3.1.1, remains unchanged. Similar to the finite-depth case, the nonlinear evolution has a slightly larger amplitude than the linear version. For the problems considered here, the weak nonlinearity has modest impact on the evolution of the linear spiral waves. We also

https://doi.org/10.1017/jfm.2026.11706 Published online by Cambridge University Press

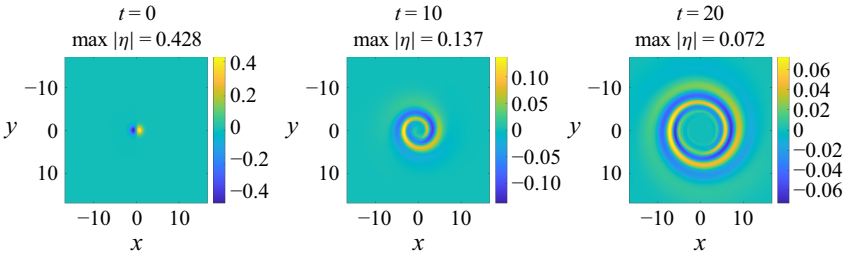


Figure 8. Evolution of the nonlinear water-wave equations (4.8) in infinite depth with initial conditions (3.4). Here $\varepsilon = 0.25$ and $\tilde{g} = 1$. This can be compared with the linear results shown in figure 4.

find numerically that adding a small amount of noise, of the order of 1 %–5 %, to the initial conditions has little effect; i.e. the spiral waves appear to be robust.

We also note the similarity between the spiral problem analysed here and the well-known problem of a small object, e.g. a pebble, thrown into still water. We refer to this as the 'pebble problem'. The only difference is that the pebble problem arises from radially symmetric initial conditions whereas spiral waves evolve from initial conditions of the form given in (3.2), e.g. those given by (3.4). This is also discussed further in Appendix A. Based on this analogy we expect the spiral waves discussed here to be observable in various settings.

5. Conclusion

Spiral waves are found in the linear and weakly nonlinear irrotational water-wave equations. These unsteady waves evolve from a suitable class of initial conditions; there is no external forcing. In the linear problem, long-time asymptotic approximations via stationary phase are found to be in good agreement with the exact solution. Numerical simulations indicate that unsteady spiral waves persist in the presence of weak nonlinearity. While spiral waves are well known in excitable media modelled by reaction–diffusion equations, they apparently have not been previously analysed in fundamental linear or nonlinear irrotational water waves. As such, these spiral phenomena are new two-space one-time dimensional solutions to the classical water-wave equations.

Funding. M.J.A. was partially supported by NSF under grant no. DMS-2306290.

Declaration of interests. The authors report no conflict of interest.

Appendix A. Initial conditions

Consider the class of dimensionless initial conditions of the form

$$\eta(x, y, t = 0) = P_1(x, y) f(r), \quad \eta_t(x, y, t = 0) = P_2(x, y) f(r), \tag{A1}$$

where $P_j(x, y)$ are suitable polynomials and $f(r)$ is a rapidly decaying radially symmetric function.

A simple case is where polynomials, P_j, are taken to be constant:

$$P_1(x, y) = A, \quad P_2(x, y) = B, \quad f(r) = \mathrm{e}^{-r^2}. \tag{A2}$$

Our initial conditions reduce down to a radially symmetric initial disturbance. This simulates the classic problem of throwing a pebble into still water which we refer to as the 'pebble problem'. In figure 9, we see the concentric ripples that emanate out from the initial disturbance as expected for the pebble problem. The stationary-phase approximation

https://doi.org/10.1017/jfm.2026.11706 Published online by Cambridge University Press

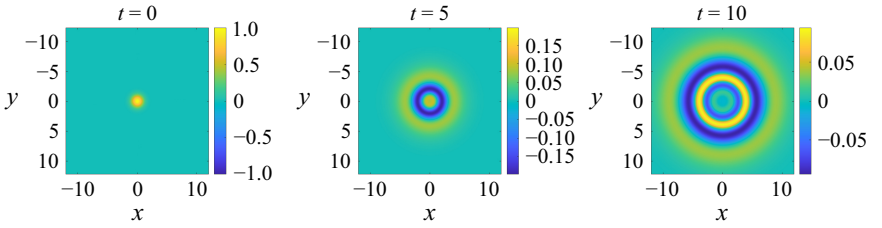


Figure 9. Evolution of the linearised water-wave equation (2.12) with dispersion relation (2.13) for radially symmetric initial conditions (A2). Here $A = 1$, $B = 0$, $h = 1$ and $\tilde{g} = 1$.

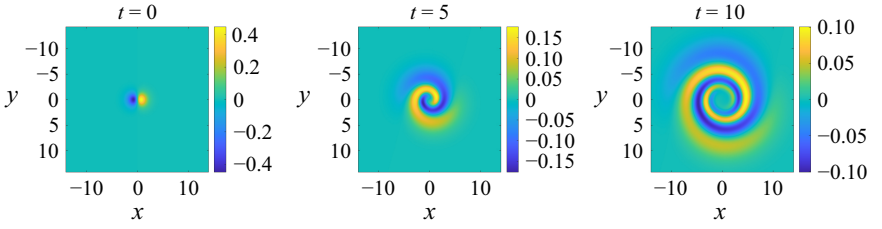


Figure 10. Evolution of the linearised water-wave equation (2.12) with dispersion relation (2.13) for exponentially decaying initial conditions (A4). Here $h = 1$ and $\tilde{g} = 1$.

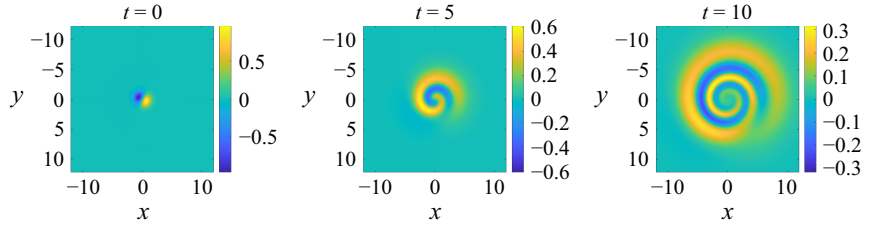


Figure 11. Evolution of the linearised water-wave equation (2.12) with dispersion relation (2.13) for skewed initial conditions given by (A5). Here $A_1 = 2$, $A_2 = 1$, $A_3 = 0$, $B_1 = 2$, $B_2 = -3$, $B_3 = 1$, $h = 1$ and $\tilde{g} = 1$.

for these radially symmetric initial conditions gives

$$\eta(\bar{r}, t) \approx \frac{\rho_0^{3/2} \mathrm{e}^{-\frac{\rho_0^2}{4}}}{4\sqrt{\bar{r}\,|\omega''(\rho_0)|\,t}} \left[\frac{A}{\omega(\rho_0)} \cos\left(\rho_0 \bar{r} t - \omega(\rho_0) t\right) - B \sin\left(\rho_0 \bar{r} t - \omega(\rho_0) t\right) \right]. \tag{A3}$$

Observe that this surface profile does not depend on θ.

Turning our attention back to the phenomena of spiral waves, we investigate two variations of the initial conditions given by (3.2):

$$P_1(x, y) = x, \quad P_2(x, y) = y, \quad f(r) = \operatorname{sech}^2(r). \tag{A4}$$

Figure 10 shows that core shape of the spiral remains unchanged and only the envelope over the spiral differs. In fact, this will be true for any $f(r)$ that decays sufficiently fast.

Next, we consider the case of general linear polynomials P_j:

$$P_1(x, y) = A_1 x + A_2 y + A_3, \quad P_2(x, y) = B_1 x + B_2 y + B_3, \quad f(r) = \mathrm{e}^{-r^2}, \tag{A5}$$

which demonstrate that generation of spirals does not rely on any specific symmetries of the initial conditions. In figure 11, we observe a distortion of the previously shown spirals;

https://doi.org/10.1017/jfm.2026.11706 Published online by Cambridge University Press

they no longer exhibit odd symmetry in x ($x \to -x$, $\eta \to -\eta$). However, we see that the underlying shape of the spiral remains hyperbolic (see (3.29)). We note that not all choices of coefficients are expected to result in a spiral wave.

The close connection to the pebble problem along with the wide class of possible initial conditions that produce spiral waves strongly suggests that these spiral waves can be observed experimentally.

Appendix B. Numerical simulations

The numerical evolution of the nonlinear water-wave equations (4.8) is stiff due to the multiplication by nonlinear Fourier wavenumbers at high frequency ($k \gg 1$). This restriction can be reduced by introducing an integrating factor that moves the linear component into an exponential factor (see Trefethen 2000). Observe that the Fourier transform of the linear part of (4.8) can be written as

$$\frac{\partial}{\partial t}\begin{bmatrix}\widehat{\eta}\\ \widehat{q_x}\\ \widehat{q_y}\end{bmatrix} = L\begin{bmatrix}\widehat{\eta}\\ \widehat{q_x}\\ \widehat{q_y}\end{bmatrix}, \quad \text{where} \quad L = \begin{bmatrix}0 & -\dfrac{\mathrm{i}k_x\omega^2(k)}{\tilde{g}k^2} & -\dfrac{\mathrm{i}k_y\omega^2(k)}{\tilde{g}k^2}\\ -\mathrm{i}\tilde{g}k_x & 0 & 0\\ -\mathrm{i}\tilde{g}k_y & 0 & 0\end{bmatrix}. \tag{B1}$$

The eigenvalues of L are $0, \pm\mathrm{i}\omega(k)$ and have no non-zero real part, so arbitrary solutions of the linear system remain bounded for all time. The implementation of an integrating factor approach reduces computation time and improves numerical stability. The integrating factor is given by

$$\mathrm{e}^{Lt} = \begin{bmatrix}\cos(\omega t) & -\dfrac{\mathrm{i}k_x\omega\sin(\omega t)}{\tilde{g}k^2} & -\dfrac{\mathrm{i}k_y\omega\sin(\omega t)}{\tilde{g}k^2}\\ -\dfrac{\mathrm{i}\tilde{g}k_x\sin(\omega t)}{\omega} & \dfrac{k_y^2+k_x^2\cos(\omega t)}{k^2} & -\dfrac{k_xk_y[1-\cos(\omega t)]}{k^2}\\ -\dfrac{\mathrm{i}\tilde{g}k_y\sin(\omega t)}{\omega} & -\dfrac{k_xk_y[1-\cos(\omega t)]}{k^2} & \dfrac{k_x^2+k_y^2\cos(\omega t)}{k^2}\end{bmatrix}. \tag{B2}$$

The evolution of the nonlinear wave equation (4.8) employs a fourth-order Runge–Kutta method in $\boldsymbol{v}$, where

$$H_0 \equiv -\frac{1}{2\pi}\iint_{\mathbb{R}^2}\mathrm{e}^{i\boldsymbol{k}\cdot\boldsymbol{r}}\tanh(kh)\frac{\mathrm{i}\boldsymbol{k}\cdot\widehat{\nabla q}}{k}\,\mathrm{d}\boldsymbol{k}, \tag{B3a}$$

$$H_1 \equiv -\frac{1}{2\pi}\iint_{\mathbb{R}^2}\mathrm{e}^{i\boldsymbol{k}\cdot\boldsymbol{r}}\left(k\tanh(kh)\widehat{\eta H_0} + \mathrm{i}\boldsymbol{k}\cdot\widehat{\eta\nabla q}\right)\mathrm{d}\boldsymbol{k}, \tag{B3b}$$

$$\begin{bmatrix}\widehat{\eta}\\ \widehat{q_x}\\ \widehat{q_y}\end{bmatrix} = \mathrm{e}^{Lt}\boldsymbol{v}(t), \tag{B3c}$$

$$\begin{aligned}M_1 = &-\varepsilon\left(k\tanh(kh)\widehat{\eta H_0} + \mathrm{i}\boldsymbol{k}\cdot\widehat{\eta\nabla q}\right)\\ &-\varepsilon^2\left(k\tanh(kh)\widehat{\eta H_1} + \frac{k^2}{2}\widehat{\eta^2 H_0} + \frac{k}{2}\widehat{\left(\mathrm{i}\boldsymbol{k}\cdot\eta^2\nabla q\right)}\tanh(kh)\right),\end{aligned} \tag{B3d}$$

https://doi.org/10.1017/jfm.2026.11706 Published online by Cambridge University Press

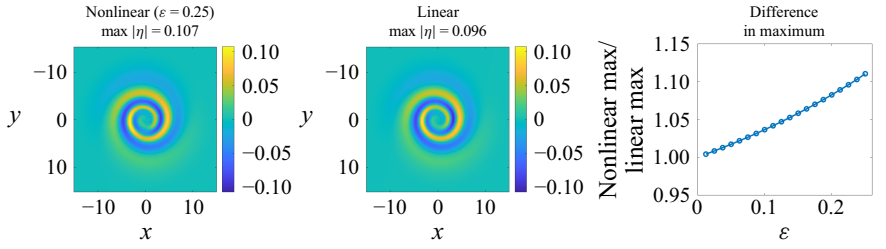


Figure 12. Comparison of the linear evolution computed exactly via Fourier transform and the evolution of the nonlinear water-wave equations (4.8) at $t = 10$; both computed with initial conditions (3.4).

$$M_2 = \mathrm{i}k_x\left(-\tilde{g}\,\widehat{\eta} + \frac{\varepsilon}{2}\left(\widehat{H_0^2} - \widehat{|\nabla q|^2}\right) + \varepsilon^2\left(\widehat{H_0 H_1} + H_0\widehat{\nabla\eta\cdot\nabla q}\right)\right), \tag{B3e}$$

$$M_3 = \mathrm{i}k_y\left(-\tilde{g}\,\widehat{\eta} + \frac{\varepsilon}{2}\left(\widehat{H_0^2} - \widehat{|\nabla q|^2}\right) + \varepsilon^2\left(\widehat{H_0 H_1} + H_0\widehat{\nabla\eta\cdot\nabla q}\right)\right), \tag{B3f}$$

$$\boldsymbol{v}_t = \mathrm{e}^{-Lt}\begin{bmatrix} M_1 \\ M_2 \\ M_2 \end{bmatrix}. \tag{B3g}$$

Figure 12 highlights the effect of the nonlinear terms on the evolution of spiral waves. Here, we evolve the water-wave equation up to time $t = 10$ for different values of ε and compare the maximum amplitude of the nonlinear spirals with their linear counterpart. We see that the core spiral structure remains unaltered with deviations in the maximum amplitude of the wave that scales linearly with ε.

References

Ablowitz, M.J. & Clarkson, P.A. 1991 *Solitons, Nonlinear Evolution Equations and Inverse Scattering*. Cambridge University Press.

Ablowitz, M.J., Cole, J.T. & Nixon, S.D. 2025 Spiral waves and localized modes in dispersive wave equations. *Wave Motion* **139**, 103579.

Ablowitz, M.J., Fokas, A.S. & Musslimani, Z.H. 2006 On a new non-local formulation of water waves. *J. Fluid Mech.* **562**, 313–343.

Ablowitz, M.J. & Haberman, R. 1975 Nonlinear evolution equations-two and three dimensions. *Phys. Rev. Lett.* **35** (18), 1185–1188.

Ablowitz, M.J., Luo, X. & Musslimani, Z.H. 2023 Six wave interaction equations in finite-depth gravity waves with surface tension. *J. Fluid Mech.* **961**, A3.

Amick, C.J., Fraenkel, L.E. & Toland, J.F. 1982 On the Stokes conjecture for the wave of extreme form. *Acta Mathematica* **148**, 193–214.

Amick, C.J. & Toland, J.F. 1981 On periodic water-waves and their convergence to solitary waves in the long-wave limit. *Phil. Trans. R. Soc. Lond. A Math. Phys. Sci.* **303** (1481), 633–669.

Beale, J.T. 1977 The existence of solitary water waves. *Commun. Pure Appl. Maths* **30** (4), 373–389.

Benjamin, T.B. & Feir, J.E. 1967 The disintegration of wave trains on deep water. Part 1. Theory. *J. Fluid Mech.* **27**, 417–430.

Benney, D.J. & Luke, J.C. 1964 On the interactions of permanent waves of finite amplitude. *J. Maths Phys. Camb.* **43** (1–4), 309–313.

Benney, D.J. & Roskes, G.J. 1969 Wave instabilities. *Stud. Appl. Maths* **48** (4), 377–385.

Berger, K.M. & Milewski, P.A. 2000 The generation and evolution of lump solitary waves in surface-tension-dominated flows. *SIAM J. Appl. Maths* **61** (3), 731–750.

Bode, M. & Purwins, H.G. 1995 Pattern formation in reaction-diffusion systems - dissipative solitons in physical systems. *Phys. D Nonlinear Phenom.* **86** (1), 53–63.

Boussinesq, J. 1871 Theorie de l'intumescence liquid appelée onde solitaire ou de translation, se propagente dans un canal rectangulaire. *C. R. Acad. Sci. Paris* **72**, 755–759.

https://doi.org/10.1017/jfm.2026.11706 Published online by Cambridge University Press

CAPASSO, V. & KUNISCH, K. 1988 A reaction-diffusion system arising in modelling man-environment diseases. *Q. Appl. Maths* **46**, 431–450.

CHEN, K.H., QIU, H.X., WU, Y., LIN, Z., HUANG, H., SHUI, L.L., DENG, D., LIU, H.Z. & CHEN, Z.G. 2021 Generation and control of dynamically tunable circular Pearcey beams with annular spiral-zone phase. *Sci. China Phys. Mech. Astron.* **64** (10), 104211.

CRAIG, W. & SULEM, C. 1993 Numerical simulation of gravity waves. *J. Comput. Phys.* **108** (1), 73–83.

CRAIK, A.D.D. 2004 The origins of water wave theory. *Annu. Rev. Fluid Mech.* **36**, 1–28.

DAVEY, A. & STEWARTSON, K. 1974 On three-dimensional packets of surface waves. *Proc. R. Soc. Lond. A* **338** (1613), 101–110.

DYACHENKO, S.A., LUSHNIKOV, P.M. & KOROTKEVICH, A.O. 2014 Complex singularity of a Stokes wave. *Sov. J. Expl Theor. Phys. Lett.* **98** (11), 675–679.

GARDNER, C.S., GREENE, J.M., KRUSKAL, M.D. & MIURA, R.M. 1967 Method for solving the Korteweg–deVries equation. *Phys. Rev. Lett.* **19** (19), 1095–1097.

GROVES, M.D. 2004 Steady water waves. *J. Nonlinear Math. Phys.* **11** (4), 435.

HAZIOT, S.V., MIKYOUNG HUR, V., STRAUSS, W., TOLAND, J.F., WAHLÉN, E., WALSH, S. & WHEELER, M.H. 2021 Traveling water waves – the ebb and flow of two centuries. arXiv e-prints arXiv: 2109.0920.

KADOMTSEV, B.B. & PETVIASHVILI, V.I. 1970 On the stability of solitary waves in weakly dispersing media. *Sov. Phys. Dokl.* **15**, 539.

KAUP, D.J. 1976 The three-wave interaction–a nondispersive phenomenon. *Stud. Appl. Maths* **55** (1), 9–44.

KENNICUTT JR., R.C. 1981 The shapes of spiral arms along the Hubble sequence. *Astron. J.* **86**, 1847–1858.

KORTEWEG, D.J. & DE VRIES, G. 1895 On the change of form of long waves advancing in a rectangular canal. *Phil. Mag.* **91** (6), 1007–1028.

LAMB, H. 1932 *Hydrodynamics*. Dover.

LIN, C.C. & SHU, F.H. 1964 On the spiral structure of disk galaxies. *Astrophys. J.* **140**, 646.

LIU, X., LUNIĆ, F., SONG, D., DAI, Z., XIA, S., TANG, L., XU, J., CHEN, Z. & BULJAN, H. 2021 Wavepacket self-rotation and helical Zitterbewegung in symmetry-broken honeycomb lattices. *Laser Photonics Rev.* **15** (7), 2000563.

LONGUET-HIGGINS, M.S. & FOX, M.J.H. 1977 Theory of the almost-highest wave: the inner solution. *J. Fluid Mech.* **80**, 721–741.

MUNK, W., ARMI, L., FISCHER, K. & ZACHARIASEN, F. 2000 Spirals on the sea. *Proc. R. Soc. Lond. A* **456** (1997), 1217.

NICOLIS, G. & PRIGOGINE, I. 1977 *Self-Organization in Nonequilibrium Systems*. Wiley.

SCHELL, A.J. & BLOEMBERGEN, N. 1978 Laser studies of internal conical diffraction II intensity patterns in an optically active crystal, alpha-iodic acid. *J. Opt. Soc. Am. (1917–1983)* **68** (8), 1098.

SHU, F.H. 2016 Six decades of spiral density wave theory. *Annu. Rev. Astron. Astrophys.* **54**, 667–724.

STOKES, G.G. 1847 On the theory of oscillatory waves. *Trans. Camb. Phil. Soc.* **8**, 441–455.

STOKES, G.G. 1880 Considerations relative to the greatest height of oscillatory irrotational waves which can be propagated without change of form. *Math. Phys. Papers* **1**, 313–343.

STRAUSS, W.A. 1977 Existence of solitary waves in higher dimensions. *Commun. Math. Phys.* **55** (2), 149–162.

TREFETHEN, L.N. 2000 *Spectral Methods in MATLAB*. SIAM.

WANG, Z. & MILEWSKI, P.A. 2012 Dynamics of gravity–capillary solitary waves in deep water. *J. Fluid Mech.* **708**, 480–501.

ZAKHAROV, V.E. 1968 Stability of periodic waves of finite amplitude on the surface of a deep fluid. *J. Appl. Mech. Tech. Phys.* **9** (2), 190–194.

ZAKHAROV, V.E. & MANAKOV, S.V. 1975 The theory of resonance interaction of wave packets in nonlinear media. *Sov. J. Expl Theor. Phys.* **42**, 842.

ZAKHAROV, V.E. & SHABAT, A.B. 1972 Exact theory of two-dimensional self-focusing and one-dimensional self-modulation of waves in nonlinear media. *Sov. J. Expl Theor. Phys.* **34**, 62.

https://doi.org/10.1017/jfm.2026.11706 Published online by Cambridge University Press